HHS Public Access

Author manuscript

J Vasc Res. Author manuscript; available in PMC 2017 February 25.

Published in final edited form as:

J Vasc Res. 2015 ; 52(5): 306–320. doi:10.1159/000443884.

Calreticulin regulates neointima formation and collagen deposition following carotid artery ligation

Kurt A. Zimmerman[1], **Dongqi Xing**[2], **Manuel A. Pallero**[1], **Ailing Lu**[1], **Masahito Ikawa**[5], **Leland Black**[3], **Kenneth L. Hoyt**[2,*], **Janusz H. Kabarowski**[3], **Marek Michalak**[4], and **Joanne E. Murphy-Ullrich**[1]

[1]Department of Pathology, University of Alabama at Birmingham, Birmingham, AL 35294-0019

[2]Department of Medicine, University of Alabama at Birmingham, Birmingham, AL 35294-0019

[3]Department of Microbiology, University of Alabama at Birmingham, Birmingham, AL 35294-0019

[4]Department of Biochemistry, University of Alberta, Canada

[5]Animal Resource Center for Infectious Disease, Research Institute for Microbial Disease, Osaka University, Japan

Abstract

Background/AIMs—The endoplasmic reticulum (ER) stress protein, calreticulin (CRT), is required for TGF-β stimulated extracellular matrix (ECM) production by fibroblasts. Since TGF-β regulates vascular fibroproliferative responses and collagen deposition, we investigated the effects of CRT knockdown on vascular smooth muscle cell (VSMCs) fibroproliferative responses and collagen deposition.

Methods—Using a carotid artery ligation model of vascular injury, Cre-recombinase-IRES-GFP plasmid was delivered with microbubbles (MB) to CRT floxed mice using ultrasound to specifically reduce CRT expression in the carotid artery.

Results—In vitro, Cre-recombinase mediated CRT knockdown in isolated floxed VSMCs decreased CRT transcript and protein, and attenuated induction of collagen I protein in response to TGF-β. TGF-β stimulation of collagen I was partly blocked by the NFAT inhibitor 11R-VIVIT. Following carotid artery ligation, CRT staining was upregulated with enhanced expression in the neointima by 14–21 days post-injury. Furthermore, Cre-recombinase-IRES-GFP plasmid delivered by targeted ultrasound reduced CRT expression in the neointima of CRT floxed mice and led to a significant reduction in neointima formation and collagen deposition. Neointimal cell number was also reduced in mice with local, tissue-specific knockdown of CRT.

Conclusions—This work establishes a novel role for CRT in mediating VSMC responses to injury through regulation of collagen deposition and neointima formation.

Corresponding author: Joanne E. Murphy-Ullrich, PhD, Department of Pathology, G001A Volker Hall, 1720 2ND AVE S, Birmingham, AL 35294-0019, murphy@uab.edu, 205-934-0415.

*current address: Department of Bioengineering, The University of Texas at Dallas, Richardson, TX 75080

Disclosures: There are no conflicts of interest.

Keywords

calreticulin; neointima formation; collagen

Introduction

Neointimal thickening is a hallmark of vascular responses to injury, both in acute injury following percutaneous coronary intervention and in response to chronic vascular injury in atherosclerosis. Neointima formation is characterized by medial vascular smooth muscle cell (VSMC) proliferation and migration from the media to the neointima and by acquisition of the synthetic phenotype with enhanced expression of extracellular matrix (ECM) components, including type I collagen, leading to vessel occlusion [1–3].

TGF-β is increased following vascular injury and plays a role in neointima formation [4]. Canonical TGF-β signaling occurs following TGF-β binding to the type II-type I receptor complex leading to phosphorylation of Smad2/3, complex formation with Smad 4, and migration into the nucleus to regulate gene transcription. Introduction of a plasmid encoding TGF-β or recombinant TGF-β enhances ECM production by VSMCs and promotes intimal thickening [5, 6]. Furthermore, blockade of TGF-β with antibodies or a soluble TGF-β decoy receptor significantly attenuated neointima formation [7, 8]. Blockade of TGF-β induced Smad signaling using adenoviral delivery of inhibitory Smad 7 attenuates neointimal formation and collagen production [9]. The role of TGF-β in VSMC proliferation is more controversial. Halloran et al. demonstrated that TGF-β inhibits human arterial SMC proliferation [10], whereas others showed that TGF-β stimulates VSMC proliferation through Smad3 and ERK-dependent pathways [11, 12].

Endoplasmic reticulum (ER) stress is becoming appreciated as an important factor in fibroproliferative disease, including vascular disease [13–15]. Calreticulin (CRT) is a calcium binding protein in the ER lumen that regulates ER calcium stores and downstream calcium-dependent signaling pathways and it also regulates protein folding as part of the CRT-calnexin pathway, acts as a chaperone, and participates in the unfolded protein response [16–18]. CRT is upregulated in the aortic arch of streptozotocin treated hamsters and in the endothelium and media of atherosclerotic arteries of rabbits fed a high fat diet [19, 20]. CRT is critical for development of fibrotic disease in multiple organs. CRT is upregulated in the unilateral ureteral obstruction model of tubulointerstitial fibrosis [21]. Mice heterozygous for CRT have reduced collagen production following unilateral ureteral obstruction-induced injury as compared to wild type mice [22]. CRT can also regulate SMC proliferation as siRNA knockdown of CRT inhibited PDGF-bb stimulated bronchiolar SMC proliferation [23]. Furthermore, our lab established that CRT is a critical regulator of ECM production in response to TGF-β, establishing a key mechanistic link between ER stress and fibrosis [24, 25]. Mouse embryonic fibroblasts from CRT null mice from have reduced type I and type III collagen and fibronectin transcript and protein [24]. In addition, cells deficient in CRT are unable to induce ECM production in response to TGF-β, even in the presence of enhanced ER stress and active Smad signaling [25]. CRT regulates TGF-β stimulated ECM production through control of ER calcium release and downstream activation of calcineurin/NFAT

signaling [25]. Inhibition of calcineurin/NFAT signaling impaired TGF-β stimulated ECM production in several fibroblast cell lines, illustrating the importance of CRT mediated calcineurin/NFAT signaling in TGF-β induced ECM production [25].

Genetic deletion of the CRT gene (*calr*) results in embryonic lethality; therefore, it has been difficult to experimentally determine the role of CRT in disease in adult animals. In our current studies, we used the carotid artery ligation mouse model of acute vascular injury in newly available CRT floxed mice to determine whether CRT is involved in regulating vascular responses to injury and neointima formation [26–28]. We used a targeted ultrasound (US) approach to deliver cre-recombinase plasmid with microbubbles (MB) to the carotid arteries of CRT floxed mice to knockdown CRT expression specifically in this tissue [29–34]. We observed that knockdown of CRT in the carotid artery significantly reduces neointima formation and neointimal collagen [27]. This study demonstrates that CRT has an important role in regulating VSMC responses to acute injury and suggests the potential utility of targeting CRT for treatment of vascular disease.

Materials and Methods

Chemicals and reagents

Dulbecco's modified Eagle's medium (DMEM) with 1 g/liter glucose was purchased from Invitrogen (Madison, WI). Protease inhibitor cocktail and ionomycin (cat# I0364) were purchased from Sigma (St. Louis, MO). D-PBS was purchased from Cellgro (Manassas, VA). 11R-VIVIT was purchased from CalBiochem (Billerica, MA). TGF-β was purchased from R&D Systems (Minneapolis, MN). Rabbit anti-β-tubulin (cat # 9104) was purchased from Santa Cruz Biotechnology (Santa Cruz, CA). Rabbit anti-collagen type I IgG (cat # 203002) was purchased from MDBioproducts (St. Paul, MN). Rat anti-mouse Platelet endothelial cell adhesion molecule 1 (PECAM1, cat # 550274) was purchased from BDbiosciences (San Jose, CA). Goat anti-calreticulin (cat# MBS222424) was purchased from MYBioSource (San Diego, CA). Rabbit monoclonal antibody to calreticulin (EPR3925) was purchased from Abcam (Cambridge, MA). Rabbit anti-Ki67 (cat # ab15580) and rabbit anti-GFP (Abcam #6556) was purchased from Abcam (Cambridge, MA). Goat anti-rat Alexa Fluor 488 (Cat # A-11006) and donkey anti-goat Alexa Fluor 555 (Cat # A-21432) conjugated secondary antibodies were purchased from Invitrogen (Carlsbad, CA). Peroxidase conjugated AffiniPure rabbit anti-goat IgG (Cat # 305-035-003) and goat anti-rabbit IgG (111-035-003) secondary antibodies were purchased from Jackson ImmunoResearch Laboratories (West Grove, PA). Biotinylated rabbit anti-goat IgG (cat # BA-5000) and goat anti-rabbit (cat # BA-1000) secondary antibodies, hematoxylin QS (cat# H-3404), VectaMount permanent mounting medium (cat # H-5000), Vectastain ABC kit (cat # PK-6100), and DAB peroxidase substrate kit (cat # SK-4100) were purchased from Vector Laboratories (Burlingame, CA). Western Lightning Chemiluminescence Reagent Plus was purchased from PerkinElmer Life Sciences (Waltham, MA). pEGFP-N1 (cat # 6086-1) and pCAG-Cre-recombinase-IRES2-GFP (Plasmid # 26646) were purchased from Clonetech (Mountain View, CA) and Addgene (Cambridge, MA) respectively. GFP (Invitrogen; Madison, WI) or Cre-recombinase-IRES-GFP (Addgene, Cabmridge, MA; Woodhead, 2006) plasmids were purchased, grown in *E. coli* (DH5α), and purified using a Qiagen

Gigaprep kit. Celltiter 96 AQueous cell proliferation assay was purchased from Promega (Madison, WI; cat # G3581). OPTISON microbubbles (MB) were purchased from GEHealthcare (St. Louis, MO).

CRT floxed mice

All protocols were approved by the Institutional Animal Care and Use Committee at the University of Alabama at Birmingham and were consistent with the Guide for the Care and Use of Laboratory Animals published by the National Institutes of Health. CRT floxed mice on the B6D2F1 background were generated by Ikawa et al [35]. Ten to 14-week-old CRT floxed mice were maintained at constant humidity (60 ± 5%), temperature (24 ± 1°C), and light cycle (6:00 A.M. to 6:00 P.M.). Mice were fed a standard pellet diet ad libitum. The presence of loxP sites in male and female breeders was confirmed by PCR (Supplemental Figure 1). Functionality of loxP sites were confirmed by using Cre-recombinase-IRES-GFP to knockout CRT in cells receiving the plasmid (Figure 1A, B).

Plasmid delivery via targeted ultrasound treatment with microbubble injection

CRT floxed mice were injected via tail vein with a solution containing 200 μL OPTISON MBs (~ 1.2×10^8 MBs) and either 300 μg GFP plasmid or 300 μg Cre-recombinase-IRES-GFP plasmid in a total volume of 250 μl (n=7 mice/group). As a technical control for the effects of US, mice were injected with Cre-recombinase-IRES-GFP with MB but in the absence of US treatment (n=3). In pilot studies, plasmid was delivered with 50 μl of OPTISON MB. Immediately following tail vein injection, ultrasound was performed on both carotid arteries. As previously detailed [36], the custom experimental ultrasound (US) setup involved single element (0.75 inch) immersion transducer (Olympus, Waltham, MA) in series with a signal generator (AFG3022B, Tektronix, Beaverton, OR) and power amplifier (A075, Electronics and Innovation, Rochester, NY). This study was completed using the following acoustic parameters: 1.0 MHz ultrasound frequency, 0.7 MPa peak negative pressure, 30 sec pulse repetition period, and 2 min duration of exposure.

GFP plasmid delivery pilot study

To determine the effectiveness of plasmid delivered using targeted US, CRT floxed mice injected with 300 μg GFP plasmid and MB (150 μl total) were subjected to US targeting the carotid arteries as above. Arteries were harvested 1, 3, 7, and 14 days following plasmid/MB injection with US treatment. Mice (n=2/group) were euthanized, perfused with PBS, and the carotid arteries harvested and frozen in OCT. Longitudinal cryostat sections of the right carotid artery were fixed with acetone and then immunostained for GFP or PECAM1. Sections were blocked with filtered PBS containing 4% BSA and 2% mouse serum followed by rabbit anti-GFP (1:500) and rat anti-PECAM1 (1:100) diluted in blocking buffer. After overnight incubation, sections were washed with PBS and incubated with goat anti-rabbit Alexa Fluor 555 (1:500) or goat anti-rat 488 (1:500) secondary antibodies for 1 hour at room temperature. Sections were washed in PBS and stained with Hoechst dye to stain DNA, a nuclear marker, for 5 minutes. Coverslips were mounted with Fluoromount-G mounting media and stored at 4 C. Vessel images were obtained using a 40X objective.

Carotid artery ligation

One week following US delivery of plasmid with microbubbles, mice were anesthetized with1.5% isofluorane in oxygen and the right common carotid artery was exposed through a midline cervical incision and ligated with a 6-0 silk suture just proximal to the bifurcation as previously described [37]. The left carotid was not ligated and served as an internal control.

Carotid Artery Harvesting and Morphometric Analysis

Three weeks following carotid ligation, mice were anesthetized with ketamine (80 mg/kg IP; Abbott Laboratories, Abbott Park, IL) and xylazine (5 mg/kg IP; Rompun, Bayer Corp; Leverkusen, Germany). The vasculature was immediately flushed with 0.01M sodium phosphate buffer (pH 7.4) and perfused with 10% formalin. Both carotid arteries were excised, fixed in 10% formalin for 24 hours, embedded in paraffin, and sectioned. Representative serial sections were stained with hematoxylin and eosin (H&E) and examined under a light microscope to locate the ligation site. Then additional sections of the artery taken 350, 500, and 700 μm proximal to the ligation site were identified and treated with Verhoeff's elastin stain to visually enhance the elastic laminae.

Three tissue sections corresponding to the upper, middle and lower portion of the carotid from each mouse were used for immunohistochemistry staining and determination of GFP or CRT expression. Computer-assisted morphometric analysis of digitized images captured from each arterial section was performed with Image J analysis software. Measurements of the 3 sections obtained for each vessel were averaged for statistical purposes. The cross-sectional area of the media, i.e. the zone bounded by the external elastic lamina and the internal elastic lamina, and the area of the intima, i.e. the zone between the internal elastic lamina and the lumen, were calculated using image J. All measurements were performed by a single examiner blinded to the treatment group.

CRT expression following carotid injury

To determine CRT expression in the vasculature following carotid artery ligation, the right common carotid arteries of CRT floxed mice were ligated as described above. Carotid arteries were harvested on days 3, 7, 14 and 21 following ligation (n=3, days 3–14, n=4, day 21). Formalin-fixed vessels were sectioned and immunostained for CRT using the rabbit monoclonal anti-CRT antibody as described below.

Isolation of CRT floxed mouse vascular smooth muscle cells (VSMCs)

Mouse VSMCs were isolated from CRT-floxed mice as previously described [38]. Briefly, mouse aortas were harvested, adventitia removed, and cells were digested with 1X collagenase for 30 minutes. The aorta was cut in to 1 mm pieces and cells were allowed to grow out of the explant for two weeks in low (1 g/L) glucose DMEM with 10% FBS. Cell outgrowths were removed and passaged using trypsin. For all experiments, cells were used between passages 3–7.

Knockdown of CRT in CRT-floxed VSMCs

CRT floxed VSMCs (500,000 cells) were transfected via nucleofection using the primary VSMC Nucleofector Kit from Amaxa Biosystems (Amaxa GmbH, Lonza) in an Amaxa Nucleofector II using program P-024. Transfected cells were cultured in DMEM (1g/L glucose) with 10% FBS for 24 hours. After 24 hours, media was switched to serum free media for 24 hours, followed by treatment with 100 pM TGF-β for 48 hours.

Immunoblotting

Following treatment, cells were harvested using 1X Laemmli lysis buffer (Bio-Rad, Hercules, CA) containing 1X protease inhibitor cocktail (Sigma cat # p8340). Cells were sonicated for 7 seconds, 5% final concentration of β-mercaptoethanol was added and samples boiled at 100 °C for 7 minutes. Samples were centrifuged and equal volumes were loaded in to 4–15% SDS-polyacrylamide gels. After separation by SDS-PAGE, samples were transferred onto a PVDF membrane at 100 volts for 100 minutes. Following transfer, membranes were blocked with 1% casein followed by application of the primary antibody. Membranes were washed in TBS-T (0.05% Tween) and secondary antibody was applied for 1 hour at room temperature. Membranes were washed with TBS-T and developed using Western Lightning Chemiluminescence Reagent Plus. Membranes were probed with rabbit anti-β-tubulin IgG to normalize for cell protein. Densitometric analyses of immunoblots were performed using the NIH Image J program. Data are expressed as the mean band density normalized for cell protein from at least three separate experiments +/− S.D.

Quantitative Real Time PCR

Cells were grown overnight in complete media containing 10% FBS and grown in serum free media for 72 hours. After treatment, RNA was harvested with TRIZOL reagent and isolated according to manufacturer's specification. Quantitative real time PCR was performed using standard protocols with an Opticon instrument (MJ Research, model CFD-3200, Quebec, Canada). Primers for *Calr* (Cat # QT00101206) and *S9* (Cat # PPM03695A) were purchased from Qiagen and verified by melt curve analysis. Transcript levels were assayed using SYBR green (Qiagen; Venlo, Netherlands). Results were calculated using the ΔΔCT method and are expressed as the mean +/− S.D. of three samples each assayed in triplicate as indicated in figure legends. Results are representative of at least 3 separate experiments.

Immunohistochemistry

Formalin fixed paraffin embedded carotid artery sections were used for immunohistochemistry. Briefly, antigen retrieval was performed on deparaffinized slides using 10 mmol/L sodium citrate buffer (pH 6.0) in a 100°C water bath for 20 minutes followed by cooling for 20 minutes. Endogenous peroxidase activity was quenched with 1% hydrogen peroxide in PBS. Tissues were blocked with 2% normal horse serum (Sigma) for 30 min. Slides were incubated with rabbit monoclonal anti-CRT IgG (1:1000) or rabbit anti-Ki67 IgG (1:1000) diluted in PBS with 2% horse serum and 0.1% Triton X-100 overnight at 4°C. Sections incubated with non-immune IgG served as a negative control. After washing in PBS with 0.1% Tween-20, appropriate biotinylated secondary antibodies (Vector

Laboratories, Burlingame, CA) (biotinylated goat anti-rabbit IgG (1:250)) were applied to the tissue for 1 hour at room temperature, followed by HRP-conjugated streptavidin (ABC kit, Vector Laboratories, Burlingame, CA) for 1 hr at room temperature at dilutions recommended by the manufacturer. Processed sections were developed with 3,3′-diaminobenzidine hydrochloride (DAB) (Vector Laboratories, Burlingame, CA) and then were counterstained with hematoxylin QS (Vector Laboratories, Burlingame, CA). After dehydration, the slides were mounted in VectaMount mounting medium (Vector Laboratories, Burlingame, CA). Images of CRT stained sections were taken using a Zeiss Axiovert 10 inverted microscope and positive stain determined using Metamorph Imaging Software. Specificity of the rabbit monoclonal antibody to CRT was confirmed by immunoblot of cell lysates from wild type and calreticulin null mouse embryonic fibroblasts (Supplemental Figure 2).

For analysis of CRT stain in the paraffin embedded sections, images were obtained with a 20X objective and total cellular CRT stain in the neointima and medial area quantified using Metamorph Imaging Software. To normalize CRT stain to neointimal area, neointimal area for each section was calculated using image J software. Analysis was performed on all mice involved in the study.

For analysis of Ki67 positive nuclei, images of the entire neointima were taken and the number of Ki67 positive cells in each neointima was counted and divided by the total number of nuclei. For each field of view, at least 100 total nuclei were counted. The observed was blinded to the treatment groups.

Trichrome Stain and Verhoeff's elastin stain—Trichrome stain and Verhoeff's elastin stain were performed by the Comparative Pathology Laboratory core facility according to standard procedures.

Statistics

The one way ANOVA of rank sums was used to analyze data with multiple groups and the Student's t-test was used to compare means between two groups. For animal studies, data were analyzed using Mann-Whitney U rank sum test. For in vitro studies, Students t-test was used to compare two groups and one way ANOVA was used to compare multiple groups. SigmaStat and GraphPad Prism were used for statistical analyses. Results were considered significant if $p<0.05$.

Results

Cre-recombinase-IRES-GFP plasmid reduces CRT transcript and protein in VSMCs from CRT floxed mice

Mice with the *calr* gene flanked by LoxP sites at exons 4 and 7 were generated as described [35]. PCR was performed on DNA from wild type and CRT floxed mice using primers specifically designed to detect the presence of LoxP sites. DNA isolated from CRT floxed male and female mice generated a 400 base pair band with the CRT floxed primers, whereas no band was produced with DNA isolated from wild type mice (Supplemental Figure 1). VSMCs isolated from CRT floxed mice were transfected with GFP or cre-recombinase-

IRES-GFP plasmid and levels of *Calr* transcript or protein determined 72 or 96 hours post transfection, respectively. Transfection with cre-recombinase-IRES-GFP reduced *Calr* transcript and protein by ~60% (Figure 1A, B) confirming that excision of exons 4–7 of CRT ablates CRT protein expression in transfected cells.

Knockdown of CRT in VSMCs significantly impairs TGF-β stimulated collagen production

CRT is a critical regulator of TGF-β stimulated ECM production including collagen and fibronectin in fibroblasts [25]. Therefore, we investigated the effect of CRT knockdown on TGF-β induced collagen production in VSMCs isolated from CRT floxed mice. Delivery of cre-recombinase-IRES-GFP to CRT floxed VSMCs reduced CRT expression by 40% and significantly attenuated TGF-β stimulated collagen production (Figure 1C).

TGF-β stimulation of collagen protein in VSMCs is partially NFAT dependent

CRT regulates TGF-β stimulated ECM production in fibroblasts through control of calcineurin/NFAT signaling [25]. Calcineurin is a serine-threonine phosphatase responsible for dephosphorylation of the transcription factor NFAT, allowing NFAT to translocate to the nucleus [17]. Inhibition of calcineurin/NFAT signaling with 11R-VIVIT, a cell permeable peptide which blocks calcineurin binding to NFAT, blocked increases in TGF-β stimulated collagen and fibronectin transcripts in fibroblasts [39]. In CRT floxed VSMCs treated with 11R-VIVIT, TGF-β stimulation of type I collagen protein was reduced by ~50% (Figure 2A). 11R-VIVIT also completely inhibited TGF-β stimulated *Col1a1* transcript and protein in rat VSMCs (Supplemental Figure 3). CRT regulation of TGF-β collagen stimulation occurs appears to occur through similar mechanisms in both fibroblasts and VSMCs.

CRT expression and collagen is upregulated in the neointima following carotid artery ligation

These studies in isolated VSMCs suggest that CRT regulates TGF-β stimulation of collagen I production. As TGF-β regulates VSMC mediated ECM production and neointimal hyperplasia in vivo [5, 6], we asked whether CRT expression is altered following acute vascular injury in the carotid artery ligation model. In the uninjured artery, intracellular CRT expression is limited to the media and endothelium (data not shown). At day 3 following injury, CRT expression is primarily in the endothelium and adventitia with minimal staining in the medial layer (Figure 3A). By day 7, neointimal formation is beginning and CRT staining is observed in these regions. At days 14 and 21, neointimal formation is robust and CRT expression is strong in the neointima (Figure 3A). Medial expression of CRT is also increased, but to a lesser extent than in the neointima. The expression of fibrillary collagens as detected by the Masson's trichrome stain shows a similar increase in neointimal collagens at days 14 and 21 (Figure 3B). These results suggest that CRT expression is elevated in regions of vascular remodeling in which fibrillary collagen expression is upregulated.

Targeted US can deliver plasmid to the vascular wall

siRNA, therapeutic drugs, or plasmid DNA can be selectively delivered to tissues through use of microbubbles (MB) with targeted ultrasound (US), which effectively transfects cells in targeted areas via sonoporation [29–34]. Ultrasound triggers expansion and compression

of gas-filled, albumin-shelled microbubbles (OPTISON), thereby generating microjets capable of inducing shear stress and membrane pores which facilitate plasmid delivery [40, 41]. In pilot studies, we delivered 300 μg of GFP plasmid mixed with MB via US targeted delivery to the carotid artery of uninjured CRT floxed mice and examined GFP expression in the carotid arteries at 1, 3, 7, or 14 days following treatment by immunofluoresence (Figure 4). Expression of GFP in the media was observed at day 1 following plasmid delivery with maximal expression at day 3. Medial staining for GFP was detectable for at least 14 days. These studies indicate that delivery of plasmid to the vascular wall is feasible through targeted ultrasound. Therefore, delivery of plasmid with MB and US treatment was conducted 7 days prior to carotid artery ligation to ensure reduction in CRT protein prior to vascular injury.

US delivery of cre-recombinase-IRES-GFP plasmid with MBs reduces neointimal CRT following carotid artery ligation

Delivery of the Cre-recombinase-IRES-GFP leads to genetic deletion of the CRT gene and persistent CRT ablation in cells receiving the plasmid. We used targeted US to deliver cre-recombinase plasmid to the carotid arteries 7 days prior to carotid artery ligation with the goal of specifically reducing medial CRT expression prior to injury. Plasmid was delivered 7 days prior to injury to ensure CRT knockdown would occur prior to injury. Carotid arteries were harvested 21 days following carotid artery ligation and sections obtained 500–550 μM from the ligation site were evaluated for CRT protein by immunohistochemistry. Strong immunostaining for CRT was observed in cells in the neointima of mice receiving GFP plasmid or cre-recombinase-IRES-GFP plasmid with MBs, but lacking US (Figure 5A). In contrast, CRT staining was markedly reduced in the neointima of carotid arteries from mice receiving the cre-recombinase-IRES-GFP plasmid with MB and US treatment (Figure 5A–C). Overall neointimal CRT was reduced by nearly 75% and by approximately 40% when normalized to neointimal area in mice receiving cre-recombinase-IRES-GFP compared to mice receiving GFP control plasmid (Figure 5B, C). Because there was a slight, but not significant, reduction in cellular CRT staining in mice receiving Cre-recombinase-IRES-GFP with MB without ultrasound, we cannot rule out the possibility that there is a low level of transfection in the absence of ultrasound.

Knockdown of CRT with cre-recombinase-IRES-GFP reduces neointima formation following vascular injury

To determine the effect of CRT knockdown on neointima formation, morphometric analysis was performed on carotid artery sections three weeks following injury. The neointimal area and neointima-to-media ratio of injured vessels was reduced by 50% in mice receiving the cre-recombinase-IRES-GFP plasmid compared to mice receiving the control GFP plasmid or the Cre-recombinase plasmid with MB but no US (Figure 6A, C, D). In contrast, medial area did not differ between groups (Figure 6B). Furthermore, mice receiving cre-recombinase-IRES-GFP plasmid with MB/US had fewer cells in the neointima as compared to controls (Figure 6E).

Knockdown of CRT with cre-recombinase-IRES-GFP reduces neointimal collagen

Since CRT knockdown inhibited TGF-β stimulated collagen production in CRT floxed VSMCs, we asked whether CRT knockdown affected collagen levels in the neointima. Analysis of Masson's trichrome stained carotid artery sections showed that mice treated with cre-recombinase-IRES-GFP with MB/US displayed reduced neointimal collagen and collagen content/neointimal cell number as compared to mice treated with GFP plasmid with MB/US or cre-recombinase-IRES-GFP with MB but no US (Figure 7A–C).

Discussion

The ER stress protein CRT is involved in fibrotic disease and in atherosclerotic plaque formation. CRT is upregulated in a model of renal tubular injury which develops tubulointerstitial fibrosis [21]. Furthermore, CRT heterozygous mice have reduced fibrosis following renal tubular injury and decreased type I and III collagen, fibronectin, and TGF-β transcript [22]. Treatment of the APA (albino-panda-albino) strain of hamster with streptozotocin to induce diabetes is a model used to induce atheromatous lesions in the aortic arch: in this model, CRT expression was significantly increased and promoted atherosclerotic lesion formation, suggesting that CRT is involved in atherosclerosis [19]. We also observed strong CRT immunostaining in aortic lesions from apoE null mice, a model that develops atherosclerotic lesions upon feeding a high fat diet [42] (data not shown), and our current studies show CRT abundantly expressed in the neointima following carotid artery ligation.

We demonstrated previously that CRT is a critical regulator of TGF-β stimulated ECM production in fibroblasts, providing initial mechanistic insight into how ER stress exacerbates fibrotic disease. Our data now demonstrate that knockdown of CRT *in vivo* significantly inhibits carotid artery ligation-induced neointima formation and neointimal collagen deposition, suggesting that CRT is a critical component of vascular disease. These studies report the first *in vivo* data utilizing CRT floxed mice as a model and provide further evidence that CRT is required for progression of fibrotic disease *in vivo*. High levels of CRT staining are present in the neointima following carotid artery ligation, suggesting an important role for CRT in response to vascular injury. To our knowledge, this is the first evidence that CRT is increased in response to acute vascular injury and that CRT is playing a causal role in vascular disease.

Previously, we showed that cells deficient in CRT have attenuated TGF-β stimulated collagen and fibronectin production due to impaired TGF-β stimulated calcium release and downstream calcineurin/NFAT signaling, suggesting a mechanism by which CRT regulates fibrotic disease [25]. To address the mechanism by which CRT is regulating neointima formation and collagen deposition *in vivo*, studies were performed on VSMCs isolated from CRT floxed mice: CRT knockdown inhibited TGF-β stimulated collagen production. Furthermore, TGF-β stimulation of collagen in rat and floxed mouse VSMCs is attenuated by the NFAT inhibitor 11R-VIVIT, suggesting that CRT is regulating TGF-β induced collagen production in VSMCs through control of NFAT signaling, as in fibroblasts [25]. Consistent with this idea are observations that inhibition of NFAT activation with cyclosporine or GFP-VIVIT significantly attenuated balloon injury-induced neointima

formation in rats and that inhibition of calcineurin signaling impairs high glucose stimulated ECM production in mice [43, 44]. High glucose induced ECM production in this study was suggested to occur through release of extracellular nucleotides leading to downstream activation of the calcineurin/NFAT pathway leading to induction of the ECM protein osteopontin [44]. Interestingly, despite the inhibitory effect of calcineurin/NFAT inhibitors on TGF-β stimulated ECM production, addition of the calcium ionophore, ionomycin, at concentrations sufficient to induce NFAT reporter activity in MEFs (data not shown) was insufficient to rescue the unresponsiveness of CRT deficient MEFs to TGF-β stimulation [25]. Similar results were observed in ionomycin and TGF-β-treated CRT floxed mouse VSMCs with 40% CRT knockdown (data not shown). These data suggest while NFAT activity is required TGF-β induced ECM production, other factors regulated by CRT, likely independent of ER calcium release and NFAT activity, are also involved.

Interestingly, knockdown of CRT with Cre-recombinase-IRES-GFP reduced neointimal cell number 21 days following injury, suggesting that in addition to regulating VSMC ECM production, CRT might also regulate neointima formation through control of VSMC proliferation. However, we failed to observe differences in Ki67 positive nuclei at 21 days following injury with CRT knockdown (data not shown). Although most VSMC proliferation in the carotid artery ligation model occurs between days 7 and 14 [27], our negative data at 21 days combined with results from in vitro studies showing that CRT knockdown did not significantly alter cell proliferation in response to either 10% FBS or to the modest stimulation by TGF-β (Supplemental Figure 4), suggest that CRT does not have a major role in regulating VSMC proliferation in this model [27]. It is possible that reduced neointimal cell number is the result of impaired cell migration. This could be due to direct effects of CRT (cell surface or ER CRT) on cell migration or due to indirect effects as a result of decreased ECM expression: for example, type I collagen and fibronectin induce migration of VSMCs [22, 45–48].

Apart from its role in the ER, CRT plays important functions at the cell surface [20]. It is not known whether CRT knockdown is affecting apoptotic cell clearance by cell surface CRT in the injured carotid arteries. CRT protein infusion into the iliofemoral arteries prior to balloon injury reduced neointimal hyperplasia and medial macrophages and T cells [49]. In atherosclerotic models with reduced expression of CRT, there was impaired clearance of apoptotic bodies by macrophages, resulting in increased foam cell formation and inflammatory cytokines [50]. However, foam cell formation is not a major factor in this acute vascular injury model. Nonetheless, the role of CRT in vascular inflammation remains to be fully explored.

Genetic deletion of the *calr* gene results in embryonic lethality due altered cardiac development and embryonic fibroblasts isolated from these embryos display impaired agonist induced calcium release and NFAT nuclear translocation [18]. Therefore, it has been difficult to experimentally determine the role of CRT in disease in adult animals, although heterozygous mice are viable to adulthood [22]. Mice with homozygous floxed CRT alleles can now be used to determine cell and tissue specific roles of CRT in adult mice. Indeed, these current studies are the first to specifically target the *calr* gene in one tissue. US-targeted delivery of cre-recombinase-IRES-GFP with MBs was used to specifically target

knockdown of CRT in the carotid artery. Since the majority of cells in the neointima following injury are derived from medial VSMCs, it is conceivable that knockdown of CRT in a minority of medial cells in the uninjured media is sufficient to impact neointima formation and collagen deposition following injury. Our results clearly demonstrate that US-targeted delivery of cre-recombinase-IRES-GFP plasmid resulted in sufficient CRT knockdown to observe a biological effect. This is consistent with observations that mice heterozygous for CRT have significantly reduced fibrosis and improved kidney function in models of renal injury [22].

In conclusion, these studies establish the importance of CRT in vascular responses to injury and demonstrate that CRT is a critical regulator of neointima formation and collagen production *in vivo*.

Supplementary Material

Refer to Web version on PubMed Central for supplementary material.

Acknowledgments

Sources of Funding: AHA grant 12IRG9160008 to JEMU, NIH T32 HL007918 to KAZ and support from UAB Department of Pathology, and by a grant to MM from CIHR (MOP-15291).

We would like to thank Marie Warren for performing tail vein injections and Dr. Peter Anderson for helpful discussions. We thank Brian Halloran for assistance with Metamorph Imaging Software and analysis of IHC sections.

Abbreviations

CRT	calreticulin
VSMC	vascular smooth muscle cells
TGF-β	transforming growth factor-beta
ECM	extracellular matrix
MB	microbubbles
US	ultrasound
ER	endoplasmic reticulum

References

1. Hoffmann R, Mintz GS, Dussaillant GR, Popma JJ, Pichard AD, Satler LF, Kent KM, Griffin J, Leon MB. Patterns and mechanisms of in-stent restenosis. A serial intravascular ultrasound study. Circulation. 1996; 94:1247–1254. [PubMed: 8822976]
2. Majesky MW. Neointima formation after acute vascular injury. Role of counteradhesive extracellular matrix proteins. Texas Heart Institute journal / from the Texas Heart Institute of St Luke's Episcopal Hospital, Texas Children's Hospital. 1994; 21:78–85.
3. Chaabane C, Otsuka F, Virmani R, Bochaton-Piallat ML. Biological responses in stented arteries. Cardiovasc Res. 2013; 99:353–363. [PubMed: 23667187]

4. Majesky MW, Lindner V, Twardzik DR, Schwartz SM, Reidy MA. Production of transforming growth factor beta 1 during repair of arterial injury. J Clin Invest. 1991; 88:904–910. [PubMed: 1832175]
5. Nabel EG, Shum L, Pompili VJ, Yang ZY, San H, Shu HB, Liptay S, Gold L, Gordon D, Derynck R, et al. Direct transfer of transforming growth factor beta 1 gene into arteries stimulates fibrocellular hyperplasia. Proc Natl Acad Sci U S A. 1993; 90:10759–10763. [PubMed: 8248168]
6. Kanzaki T, Tamura K, Takahashi K, Saito Y, Akikusa B, Oohashi H, Kasayuki N, Ueda M, Morisaki N. In vivo effect of tgf- beta 1. Enhanced intimal thickening by administration of tgf- beta 1 in rabbit arteries injured with a balloon catheter. Arterioscler Thromb Vasc Biol. 1995; 15:1951–1957. [PubMed: 7583576]
7. Wolf YG, Rasmussen LM, Ruoslahti E. Antibodies against transforming growth factor-beta 1 suppress intimal hyperplasia in a rat model. J Clin Invest. 1994; 93:1172–1178. [PubMed: 8132757]
8. Smith JD, Bryant SR, Couper LL, Vary CP, Gotwals PJ, Koteliansky VE, Lindner V. Soluble transforming growth factor-beta type ii receptor inhibits negative remodeling, fibroblast transdifferentiation, and intimal lesion formation but not endothelial growth. Circ Res. 1999; 84:1212–1222. [PubMed: 10347096]
9. Mallawaarachchi CM, Weissberg PL, Siow RC. Smad7 gene transfer attenuates adventitial cell migration and vascular remodeling after balloon injury. Arterioscler Thromb Vasc Biol. 2005; 25:1383–1387. [PubMed: 15860740]
10. Halloran BG, Prorok GD, So BJ, Baxter BT. Transforming growth factor-beta 1 inhibits human arterial smooth-muscle cell proliferation in a growth-rate-dependent manner. Am J Surg. 1995; 170:193–197. [PubMed: 7631929]
11. Tsai S, Hollenbeck ST, Ryer EJ, Edlin R, Yamanouchi D, Kundi R, Wang C, Liu B, Kent KC. Tgf-beta through smad3 signaling stimulates vascular smooth muscle cell proliferation and neointimal formation. Am J Physiol Heart Circ Physiol. 2009; 297:H540–549. [PubMed: 19525370]
12. Suwanabol PA, Seedial SM, Shi X, Zhang F, Yamanouchi D, Roenneburg D, Liu B, Kent KC. Transforming growth factor-beta increases vascular smooth muscle cell proliferation through the smad3 and extracellular signal-regulated kinase mitogen-activated protein kinases pathways. J Vasc Surg. 2012; 56:446–454. [PubMed: 22521802]
13. Lenna S, Trojanowska M. The role of endoplasmic reticulum stress and the unfolded protein response in fibrosis. Curr Opin Rheumatol. 2012; 24:663–668. [PubMed: 22918530]
14. Ishimura S, Furuhashi M, Mita T, Fuseya T, Watanabe Y, Hoshina K, Kokubu N, Inoue K, Yoshida H, Miura T. Reduction of endoplasmic reticulum stress inhibits neointima formation after vascular injury. Scientific reports. 2014; 4:6943. [PubMed: 25373918]
15. Noda T, Maeda K, Hayano S, Asai N, Enomoto A, Takahashi M, Murohara T. New endoplasmic reticulum stress regulator, gipie, regulates the survival of vascular smooth muscle cells and the neointima formation after vascular injury. Arterioscler Thromb Vasc Biol. 2015; 35:1246–1253. [PubMed: 25792451]
16. Michalak M, Groenendyk J, Szabo E, Gold LI, Opas M. Calreticulin, a multi-process calcium-buffering chaperone of the endoplasmic reticulum. Biochem J. 2009; 417:651–666. [PubMed: 19133842]
17. Groenendyk J, Lynch J, Michalak M. Calreticulin, ca2+, and calcineurin - signaling from the endoplasmic reticulum. Mol Cells. 2004; 17:383–389. [PubMed: 15232210]
18. Mesaeli N, Nakamura K, Zvaritch E, Dickie P, Dziak E, Krause KH, Opas M, MacLennan DH, Michalak M. Calreticulin is essential for cardiac development. J Cell Biol. 1999; 144:857–868. [PubMed: 10085286]
19. Kurokawa M, Hideshima M, Ishii Y, Kyuwa S, Yoshikawa Y. Aortic er stress in streptozotocin-induced diabetes mellitus in apa hamsters. Exp Anim. 2009; 58:113–121. [PubMed: 19448334]
20. Gold LI, Eggleton P, Sweetwyne MT, Van Duyn LB, Greives MR, Naylor SM, Michalak M, Murphy-Ullrich JE. Calreticulin. Non-endoplasmic reticulum functions in physiology and disease. Faseb J. 2010; 24:665–683. [PubMed: 19940256]
21. Kypreou KP, Kavvadas P, Karamessinis P, Peroulis M, Alberti A, Sideras P, Psarras S, Capetanaki Y, Politis PK, Charonis AS. Altered expression of calreticulin during the development of fibrosis. Proteomics. 2008; 8:2407–2419. [PubMed: 18563736]

22. Prakoura N, Politis PK, Ihara Y, Michalak M, Charonis AS. Epithelial calreticulin up-regulation promotes profibrotic responses and tubulointerstitial fibrosis development. Am J Pathol. 2013; 183:1474–1487. [PubMed: 24035512]
23. Miglino N, Roth M, Lardinois D, Tamm M, Borger P. Calreticulin is a negative regulator of bronchial smooth muscle cell proliferation. Journal of allergy. 2012; 2012:783290. [PubMed: 22500186]
24. Van Duyn Graham L, Sweetwyne MT, Pallero MA, Murphy-Ullrich JE. Intracellular calreticulin regulates multiple steps in fibrillar collagen expression, trafficking, and processing into the extracellular matrix. J Biol Chem. 2010; 285:7067–7078. [PubMed: 20044481]
25. Zimmerman KA, Graham LV, Pallero MA, Murphy-Ullrich JE. Calreticulin regulates transforming growth factor-beta-stimulated extracellular matrix production. J Biol Chem. 2013; 288:14584–14598. [PubMed: 23564462]
26. Zhang LN, Parkinson JF, Haskell C, Wang YX. Mechanisms of intimal hyperplasia learned from a murine carotid artery ligation model. Current vascular pharmacology. 2008; 6:37–43. [PubMed: 18220938]
27. Kumar A, Lindner V. Remodeling with neointima formation in the mouse carotid artery after cessation of blood flow. Arterioscler Thromb Vasc Biol. 1997; 17:2238–2244. [PubMed: 9351395]
28. Wang X, Chai H, Lin PH, Lumsden AB, Yao Q, Chen C. Mouse models of neointimal hyperplasia. Techniques and applications. Medical science monitor: international medical journal of experimental and clinical research. 2006; 12:RA177–185. [PubMed: 16940942]
29. Hashiya N, Aoki M, Tachibana K, Taniyama Y, Yamasaki K, Hiraoka K, Makino H, Yasufumi K, Ogihara T, Morishita R. Local delivery of e2f decoy oligodeoxynucleotides using ultrasound with microbubble agent (optison) inhibits intimal hyperplasia after balloon injury in rat carotid artery model. Biochem Biophys Res Commun. 2004; 317:508–514. [PubMed: 15063786]
30. Zhou J, Wang Y, Xiong Y, Wang H, Feng Y, Chen J. Delivery of tfpi-2 using ultrasound with a microbubble agent (sonovue) inhibits intimal hyperplasia after balloon injury in a rabbit carotid artery model. Ultrasound in medicine & biology. 2010; 36:1876–1883. [PubMed: 20888684]
31. Suzuki J, Ogawa M, Takayama K, Taniyama Y, Morishita R, Hirata Y, Nagai R, Isobe M. Ultrasound-microbubble-mediated intercellular adhesion molecule-1 small interfering ribonucleic acid transfection attenuates neointimal formation after arterial injury in mice. J Am Coll Cardiol. 2010; 55:904–913. [PubMed: 20185042]
32. Phillips LC, Dhanaliwala AH, Klibanov AL, Hossack JA, Wamhoff BR. Focused ultrasound-mediated drug delivery from microbubbles reduces drug dose necessary for therapeutic effect on neointima formation--brief report. Arterioscler Thromb Vasc Biol. 2011; 31:2853–2855. [PubMed: 21960561]
33. Taniyama Y, Tachibana K, Hiraoka K, Namba T, Yamasaki K, Hashiya N, Aoki M, Ogihara T, Yasufumi K, Morishita R. Local delivery of plasmid DNA into rat carotid artery using ultrasound. Circulation. 2002; 105:1233–1239. [PubMed: 11889019]
34. Kipshidze NN, Porter TR, Dangas G, Yazdi H, Tio F, Xie F, Hellinga D, Wolfram R, Seabron R, Waksman R, Abizaid A, Roubin G, Iyer S, Colombo A, Leon MB, Moses JW, Iversen P. Novel site-specific systemic delivery of rapamycin with perfluorobutane gas microbubble carrier reduced neointimal formation in a porcine coronary restenosis model. Catheter Cardiovasc Interv. 2005; 64:389–394. [PubMed: 15736246]
35. Tokuhiro K, Satouh Y, Nozawa K, Isotani A, Fujihara Y, Hirashima Y, Matsumura H, Takumi K, Miyano T, Okabe M, Benham AM, Ikawa M. Calreticulin is required for development of the cumulus oocyte complex and female fertility. Sci Rep. 2015; 5:14254. [PubMed: 26388295]
36. Sorace AG, Korb M, Warram JM, Umphrey H, Zinn KR, Rosenthal E, Hoyt K. Ultrasound-stimulated drug delivery for treatment of residual disease after incomplete resection of head and neck cancer. Ultrasound in medicine & biology. 2014; 40:755–764. [PubMed: 24412168]
37. Hage FG, Oparil S, Xing D, Chen YF, McCrory MA, Szalai AJ. C-reactive protein-mediated vascular injury requires complement. Arterioscler Thromb Vasc Biol. 2010; 30:1189–1195. [PubMed: 20339115]
38. Ross R. The smooth muscle cell. Ii. Growth of smooth muscle in culture and formation of elastic fibers. The Journal of cell biology. 1971; 50:172–186. [PubMed: 4327464]

39. Noguchi H, Matsushita M, Okitsu T, Moriwaki A, Tomizawa K, Kang S, Li ST, Kobayashi N, Matsumoto S, Tanaka K, Tanaka N, Matsui H. A new cell-permeable peptide allows successful allogeneic islet transplantation in mice. Nat Med. 2004; 10:305–309. [PubMed: 14770176]
40. Sirsi S, Borden M. Microbubble compositions, properties and biomedical applications. Bubble science engineering and technology. 2009; 1:3–17. [PubMed: 20574549]
41. Suzuki R, Oda Y, Utoguchi N, Maruyama K. Progress in the development of ultrasound-mediated gene delivery systems utilizing nano- and microbubbles. Journal of controlled release official journal of the Controlled Release Society. 2011; 149:36–41. [PubMed: 20470839]
42. Nakashima Y, Plump AS, Raines EW, Breslow JL, Ross R. Apoe-deficient mice develop lesions of all phases of atherosclerosis throughout the arterial tree. Arterioscler Thromb. 1994; 14:133–140. [PubMed: 8274468]
43. Liu Z, Zhang C, Dronadula N, Li Q, Rao GN. Blockade of nuclear factor of activated t cells activation signaling suppresses balloon injury-induced neointima formation in a rat carotid artery model. J Biol Chem. 2005; 280:14700–14708. [PubMed: 15681847]
44. Nilsson-Berglund LM, Zetterqvist AV, Nilsson-Ohman J, Sigvardsson M, Gonzalez Bosc LV, Smith ML, Salehi A, Agardh E, Fredrikson GN, Agardh CD, Nilsson J, Wamhoff BR, Hultgardh-Nilsson A, Gomez MF. Nuclear factor of activated t cells regulates osteopontin expression in arterial smooth muscle in response to diabetes-induced hyperglycemia. Arterioscler Thromb Vasc Biol. 2010; 30:218–224. [PubMed: 19965778]
45. Nelson PR, Yamamura S, Kent KC. Extracellular matrix proteins are potent agonists of human smooth muscle cell migration. J Vasc Surg. 1996; 24:25–32. discussion 32–23. [PubMed: 8691524]
46. Orr AW, Elzie CA, Kucik DF, Murphy-Ullrich JE. Thrombospondin signaling through the calreticulin/ldl receptor-related protein co-complex stimulates random and directed cell migration. J Cell Sci. 2003; 116:2917–2927. [PubMed: 12808019]
47. Nanney LB, Woodrell CD, Greives MR, Cardwell NL, Pollins AC, Bancroft TA, Chesser A, Michalak M, Rahman M, Siebert JW, Gold LI. Calreticulin enhances porcine wound repair by diverse biological effects. Am J Pathol. 2008; 173:610–630. [PubMed: 18753412]
48. Shi F, Shang L, Pan BQ, Wang XM, Jiang YY, Hao JJ, Zhang Y, Cai Y, Xu X, Zhan QM, Wang MR. Calreticulin promotes migration and invasion of esophageal cancer cells by upregulating neuropilin-1 expression via stat5a. Clin Cancer Res. 2014; 20:6153–6162. [PubMed: 25231404]
49. Dai E, Stewart M, Ritchie B, Mesaeli N, Raha S, Kolodziejczyk D, Hobman ML, Liu LY, Etches W, Nation N, Michalak M, Lucas A. Calreticulin, a potential vascular regulatory protein, reduces intimal hyperplasia after arterial injury. Arterioscler Thromb Vasc Biol. 1997; 17:2359–2368. [PubMed: 9409202]
50. Kojima Y, Downing K, Kundu R, Miller C, Dewey F, Lancero H, Raaz U, Perisic L, Hedin U, Schadt E, Maegdefessel L, Quertermous T, Leeper NJ. Cyclin-dependent kinase inhibitor 2b regulates efferocytosis and atherosclerosis. J Clin Invest. 2014; 124:1083–1097. [PubMed: 24531546]

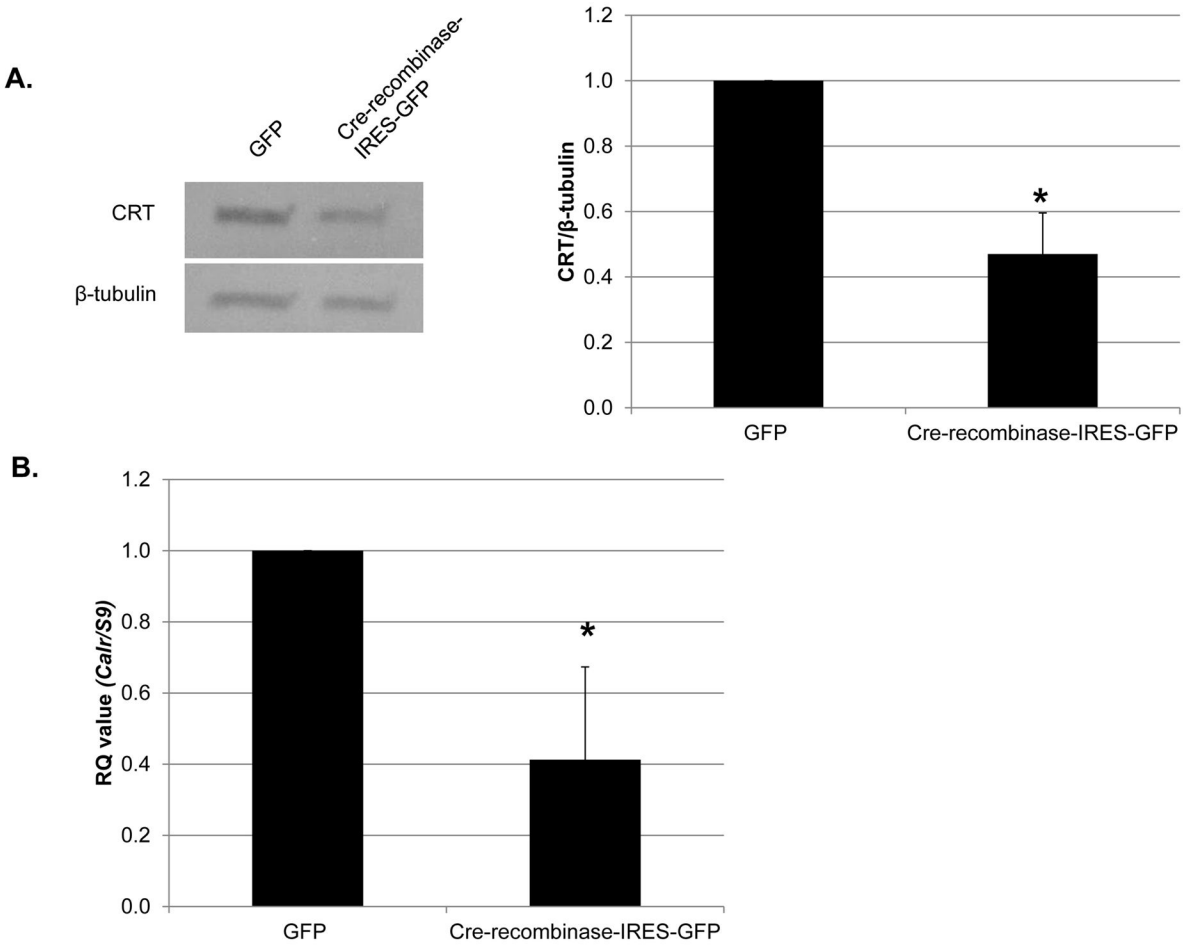

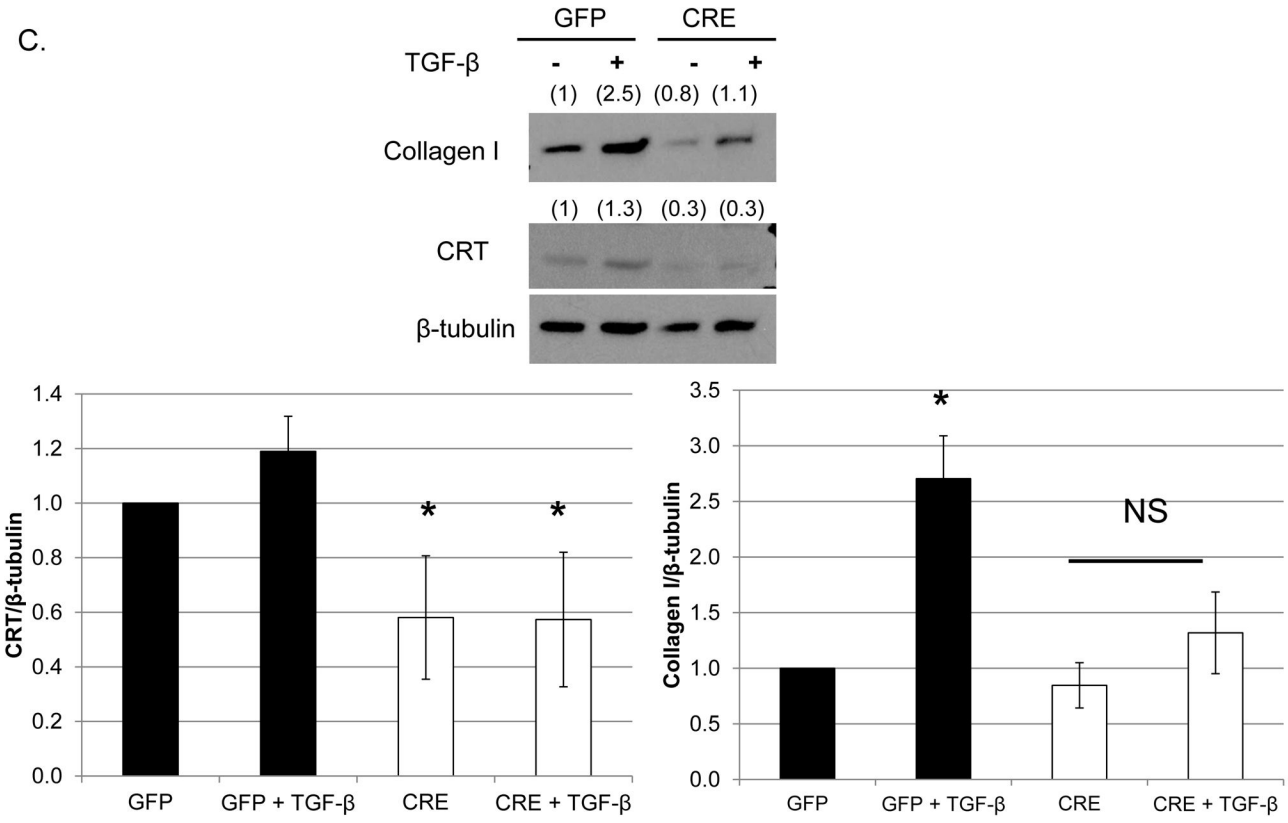

Figure 1. Knockdown of CRT in VSMCs isolated from CRT floxed mice inhibits TGF-β stimulated collagen production

(A, B) VSMCs were isolated from CRT floxed mice, transfected with 1 μg GFP or cre-recombinase-IRES-GFP, and grown overnight in media with 10% FBS. Cells were switched to serum free DMEM for the remainder of the experiment. (A) After 96 total hours, cell lysates were immunoblotted for CRT and normalized to β-tubulin. (n=3 separate experiments). A representative blot is shown in (A). (B) After 72 total hours, RNA was harvested by TRIZOL and transcript levels of C*alr* and *S9* were determined by quantitative real time PCR (n=3 separate experiments). (C) CRT floxed VSMCs were transfected with 1 μg GFP or cre-recombinase-IRES-GFP plasmid, grown overnight in DMEM with 10% FBS, and then switched to serum free DMEM for 24 hours. Cells were treated with 100 pM TGF-β for 48 hours and cell lysates immunoblotted for CRT and type I collagen. A representative blot is shown. Densitometric analyses represent mean density normalized to β-tubulin (indicated above the bands) +/− S.D. (n=3 separate experiments). *p<0.05 vs GFP transfected cells.

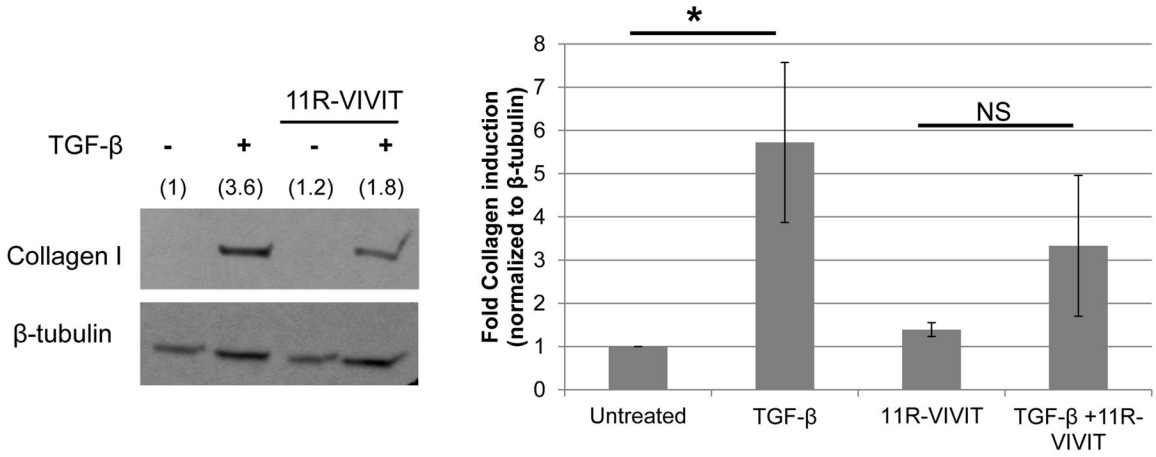

Figure 2. CRT regulates *TGF-β* stimulated collagen production in VSMCs through an NFAT-dependent manner

(A) CRT floxed VSMCs were grown overnight in DMEM with 10% FBS, switched to serum free DMEM overnight, and pretreated with 1 μM 11R-VIVIT for 60 minutes prior to adding 100 pM TGF-β. Cells were then treated daily with TGF-β +/− 11R-VIVIT peptide over 48 hours. Cell lysates were immunoblotted for type I collagen. A representative blot is shown. Bands were analyzed by densitometry and normalized to β-tubulin (indicated above band). Results are mean density normalized to β-tubulin +/− S.D. from 3 separate experiments. *$p<0.05$ vs untreated cells.

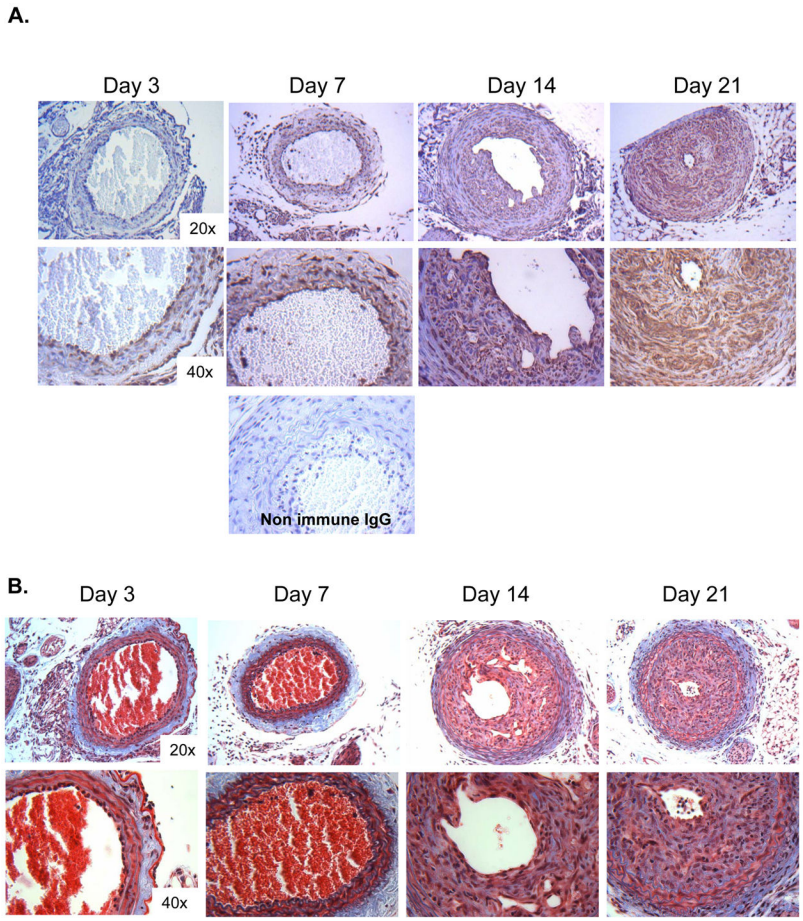

Figure 3. CRT staining and fibrillary collagens are increased in the neointima following carotid artery ligation

(A, B) Carotid artery ligation was performed on CRT floxed mice and carotid arteries were harvested 3, 7, 14, and 21 days following ligation. (A) Immunostaining for CRT was performed using a rabbit monoclonal anti-CRT antibody. Representative images depict strong CRT staining in the neointima 14 and 21 days post ligation. The original magnification of the images is 20x (top panels) and 40x (bottom panels). A control panel is shown from an artery harvested at 7 days in which non-immune rabbit IgG was used as the primary antibody. (B) Representative Masson's Trichrome stained cross sections of right carotid arteries harvested 3, 7, 14, and 21 days following ligation are shown. The original magnification of the images is 20x (top panels) and 40x (bottom panels).

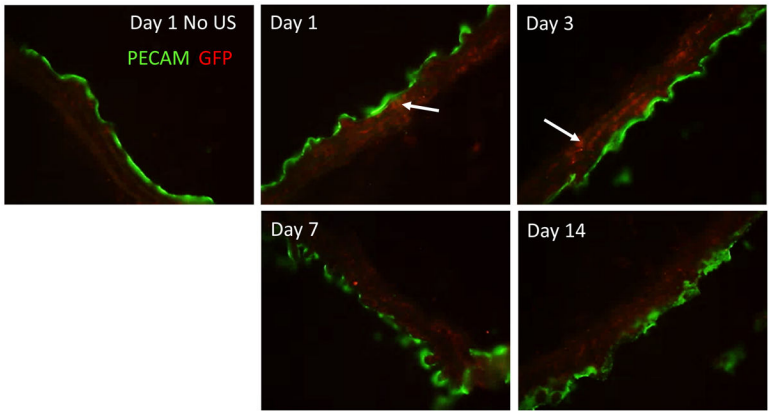

Figure 4. Delivery of GFP plasmid to medial cells by targeted ultrasound

CRT floxed mice were injected via tail vein with 300 μg GFP plasmid with MB, subjected to US and carotid arteries harvested 1, 3, 7, and 14 days following US. Injection of GFP plasmid with MB but lacking US and harvested at day 1 served as a control. Immunofluorescence for GFP (red) and PECAM1 (green) was performed on longitudinal sections and images taken at 40x. White arrows indicate individual smooth muscle cells which were transfected with the GFP plasmid. Representative images are shown.

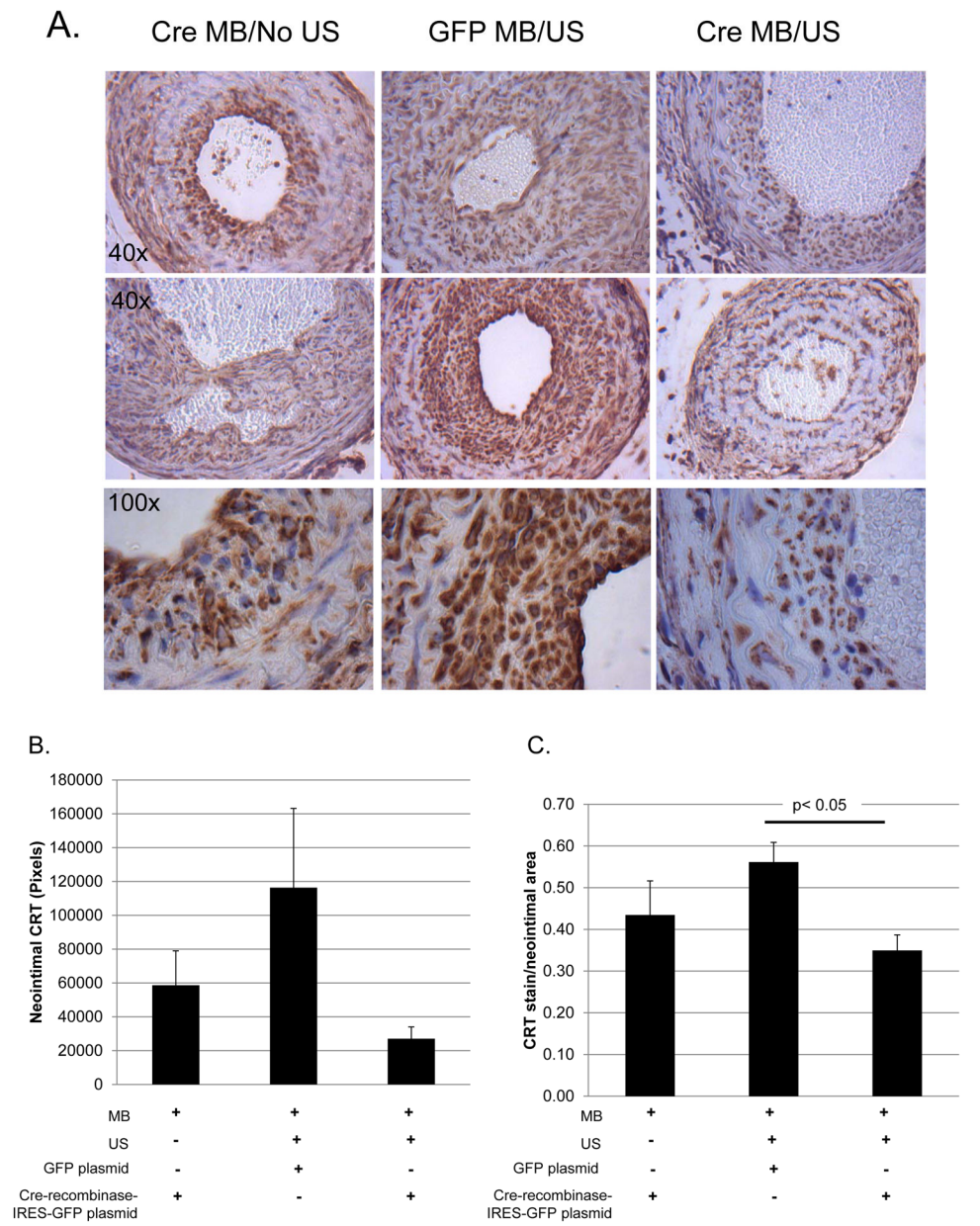

Figure 5. Delivery of Cre-recombinase plasmid to the carotid artery of CRT floxed mice reduces neointimal CRT levels

CRT floxed mice with treated with carotid artery-targeted US in the presence of MB to deliver Cre-recombinase-IRES-GFP or GFP plasmids. Cre-recombinase plasmid delivered with MB but without US (Cre MB/No US) served as an additional control. Twenty one days following carotid artery ligation, carotid arteries were perfusion fixed, embedded in paraffin, and sectioned. (A) Immunostaining for CRT was performed using the rabbit monoclonal anti-CRT antibody. Initial magnification was 40x (top, middle panel) or 100x (bottom panel). Control sections in which non-immune rabbit IgG was substituted for the primary antibody were negative (data not shown). (B, C) CRT stain was quantified using Metamorph Imaging Software: (B) total CRT stain (pixels) in the neointima (C) CRT stain normalized to

neointima area. Results are expressed as mean values +/− SEM (n=3, cre-recombinase-IRES-GFP with MB/NO US; n=7, GFP with MB/US; or n=7, Cre-recombinase-IRES-GFP with MB/US.) *p<0.05 Cre-recombinase with MB/US vs GFP plasmid with MB/US.

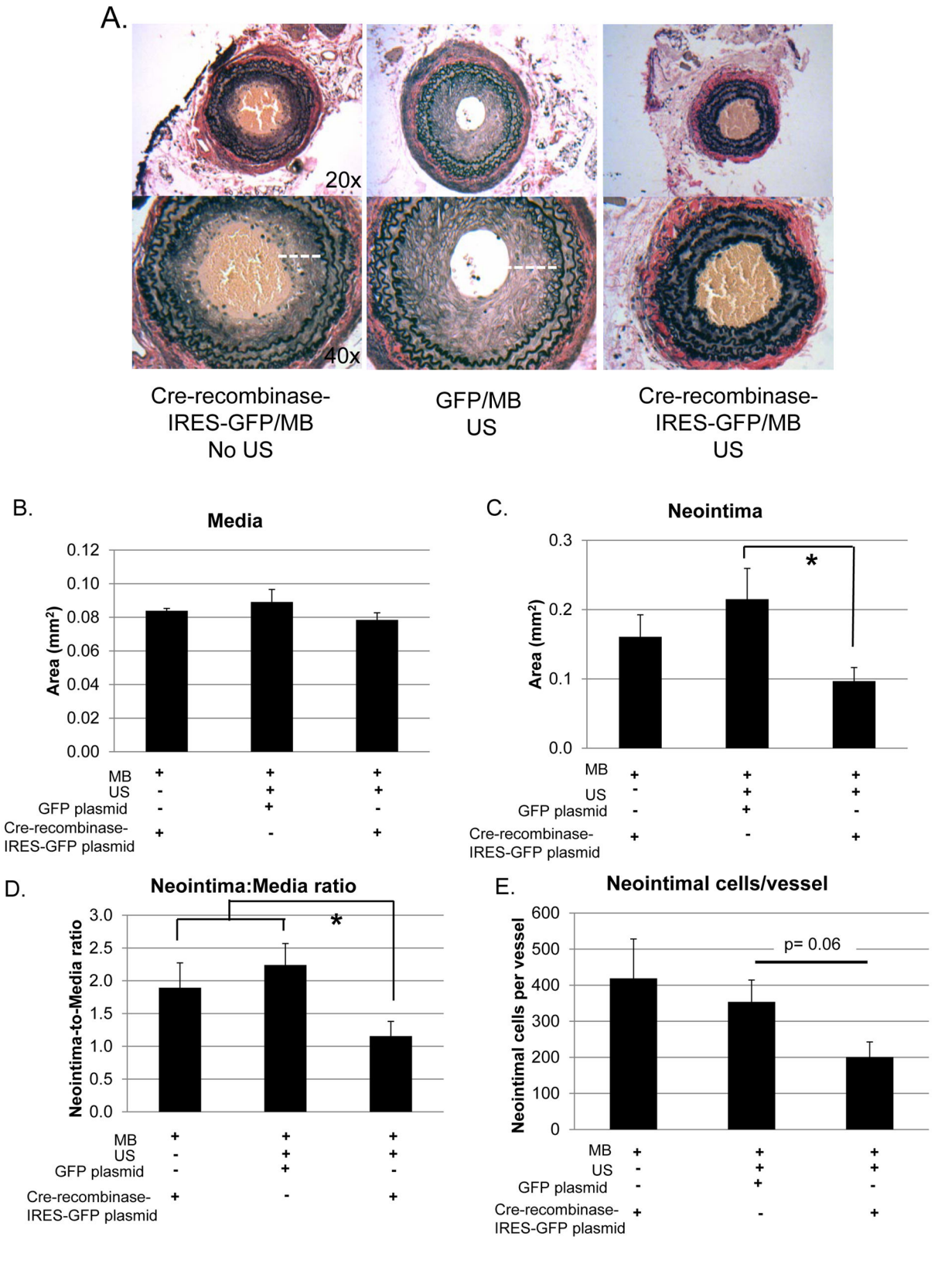

Figure 6. Neointima formation following carotid ligation is reduced in mice treated with Cre-recombinase with MB and US

Carotid arteries were harvested 21 days following ligation and subjected to analyses. (A) Representative elastin stained cross sections of right carotid arteries (original magnification 20x top panel, 40x bottom panel). Quantification of medial area (B), neointimal area (C), and neointima-to-media ratio (D) are shown. Neointima is indicated by a white dashed line in the control animals (40x images). The Cre-recombinase MB/US image (right) does not have a measurable neointima. Clots are observed in the lumens of the Cre-recombinase MB and MB/US arteries. Images quantified using NIH Image J software were obtained using a 20X objective. (E) Quantification of neointimal cell number per vessel 3 weeks following carotid artery ligation is shown. Total nuclei were counted using the 500 μm H&E stained section. Results are expressed as means +/− SEM (n=3,cre-recombinase-IRES-GFP with MB/NO US; n=7, GFP with MB and US; or n=7, Cre-recombinase-IRES-GFP with MB and US.) *$p<0.05$.

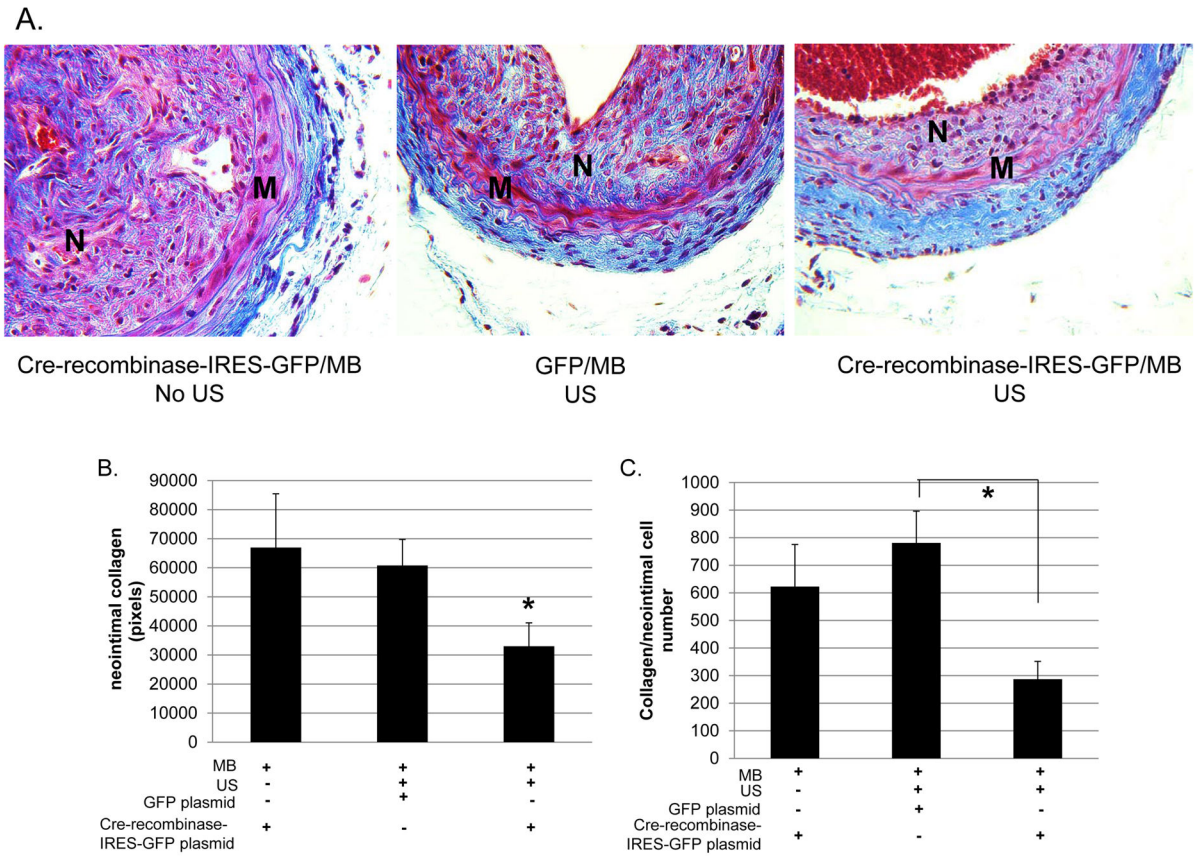

Figure 7. Neointimal collagen is reduced in mice treated with Cre-recombinase plasmid with MB and US

(A) Representative Masson's Trichrome stained cross sections of right carotid arteries 3 weeks following carotid artery ligation. (B) Quantification of total neointimal collagen content and (C) collagen content normalized to neointimal cell number were performed using Metamorph Imaging Software. Images were obtained using a 40x objective. "M" represents media and "N" represents neointima. Results are expressed as means +/− SEM (n=3, cre-recombinase-IRES-GFP with MB/NO US; n=7, GFP with MB and US; or n=7, Cre-recombinase-IRES-GFP with MB and US.) *p<0.05